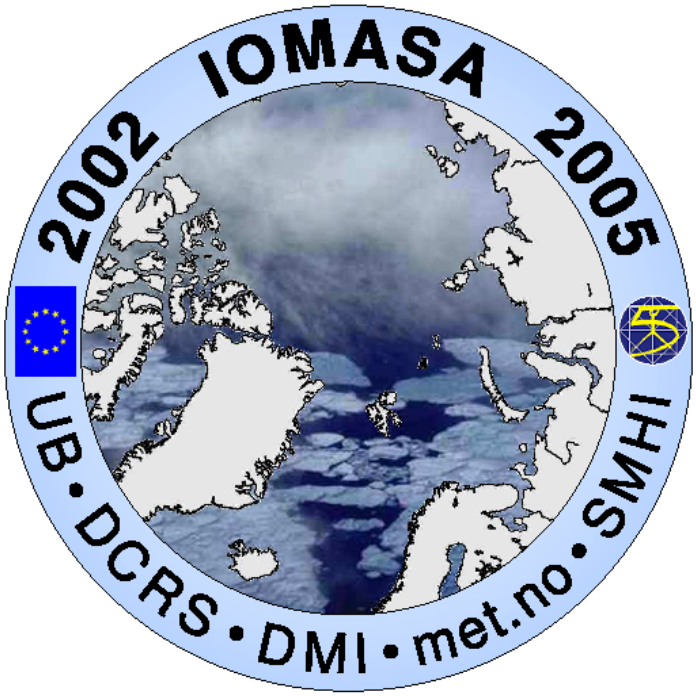

Report for IOMASA deliverable 3.2.1

Emissivity and backscatter model for sea ice

Rasmus Tonboe, Søren Andersen, Leif Toudal, & Georg Heygster

Table of contents:

This manuscript was submitted for a book on: 'Radiative transfer models for microwave radiometry', edited by C. Mätzler

1. Introduction

The strategic importance of sea ice emission models is to relate physical properties of the target to brightness temperatures (T_b) at different microwave frequencies (*?*) and polarisations and further to interpolate between observations at different places and frequencies. Because the radiances received at the satellite generally contains contributions from both atmosphere and surface, the surface emission model relationships are needed for the retrieval of both surface and atmospheric parameters. While there are physical microwave models describing the atmosphere, the open ocean and partly the land covering a wide range of microwave frequencies and polarisations, such models are generally missing for ice-covered Polar Regions. The importance of sea ice emission models is illustrated in the applications of this chapter. The aim here is to give a short overview over the quantitative influence of different microphysical parameters in sea ice and the snow on top of it at 50° incidence angle and how these link to emissivity, brightness temperature, dielectric properties and scattering using a sea ice version of MEMLS. We further present three sea ice emissivity modelling applications: sensitivity of emissivity to snow parameters at sounding frequencies, sea ice concentration estimate sensitivity to ice surface emissivity, and investigation of new sensors (i.e. SMOS) potential for sea ice mapping.

1.1. Sea ice and microwave emission measurements

Formation environment, ice cover distribution, snow cover, ice surface roughness, ice density, ice salinity and inclusion content are important properties for the understanding and interpretation of sea ice microwave data. Emission models provide a link between these physical properties and microwave measurements and thereby to the understanding of measurements. Measurements are acquired from surface based installations, aircraft or satellite. Polar orbiting satellites carrying microwave radiometers cover the globe daily with measurements and in particular, Polar Regions, several times a day. Reported sea ice measurements at different microwave frequencies cover the range from 1.4 to 183 GHz. For example, aircraft 1.4 GHz (L-band) measurements acquired recently over sea ice during summer melt (Klein et al. 2004). Eppler et al. (1992), and the references herein, describes measured sea ice emissivities between 4.9 and 94 GHz for different ice types. Hewison & English (1999) and Selbach (2003) reports millimetre wavelength measurements between 89 and 183 GHz in the Baltic and Arctic Ocean respectively. Our focus is on the frequencies: 1.4, 7, 10, 19, 23, 37, 50, 89, 157, 183 GHz, which represents channels on present and future satellite sensors (e.g. CMIS, SMOS, SSM/I, AMSR, AMSU-B). The T_b measured at these frequencies has different sensitivity to natural variability of snow and sea ice microphysical properties. The general appearance of the three predominant ice types in the Arctic: new-ice, first-year ice and multiyear ice types is distinguishable using microwave remote sensing because of differences in dielectric and scattering properties. It is therefore convenient in this investigation to distinguish between these three major classes of sea ice.

Thin ice here represented by *Nilas* belongs to the category new-ice (<10 cm). It forms under quiescent conditions. It has a smooth surface with no or little snow cover and relatively high salinity, *S*, of 14-16 psu. The density is about 920 kg/m^3 (Tucker et al., 1991). Under continued growth, nilas will form young ice and eventually first-year ice.

The level *first-year ice* (0.3-2 m) surface salinity is stable above 6 psu during winter. In fact, during winter, the level first-year ice microwave signatures change primarily due to snow cover related processes (Eppler et al., 1992). Snow cover properties directly affect T_b, e.g. liquid water content (*W*), grain size, density (*?*) etc., and indirectly by the thermodynamic control of the snow cover on the ice e.g. brine volume (Barber et al., 1995).

Multiyear ice has survived the seasonal melt. The melt processes re-crystallize the snow and ice, flush brine from the ice interior, and create surface topography i.e. melt ponds and hummocks. The hummocks are porous with large air bubbles and voids, frozen melt ponds are less porous. Salinity increases downwards with about 0.0-0.1 psu above sea level and 3.0-3.5 psu below (Weeks & Ackley, 1986). It differs from other ice types by a large number density of void scatters in the upper part of the ice, its low salinity and thickness (often several meters thick).

During summer (May-August), about half of the Arctic ice cover melts (its area shrinks from about $15x10^6$ km^2 to $6.5x10^6$ km^2) (Parkinson & Cavalieri, 1989). Melting sea ice undergoes a significant and complex transformation described in connection with microwave remote sensing by e.g. Garrity (1992) and Gogineni et al. (1992). These processes are understood relatively poorly in terms of microwave remote sensing signatures (Carsey et al., 1992). The summer season is therefore beyond the scope of the present text, which focuses on winter conditions.

1.2. Satellite radiometer field-of-view, sea ice heterogeneity and modelling

Sea ice and snow cover on sea ice is heterogeneous within the satellite field-of-view from e.g. 5 to 50 km for space borne radiometers (Eppler et al., 1992). Direct comparison between point measurements (and surface based sensors) on the ice and satellite data is therefore not feasible (Tonboe & Andersen, 2004). Satellite measurements are an ensemble average of the different emissivities present within the field-of-view and the antenna gain pattern. Models compute emissivities of laterally homogeneous structures of snow and sea ice. Therefore, comparison between emission models and brightness temperature measurements is possible only on local scales where snow and sea ice is laterally homogenous. These comparisons can be done with laboratory measurements (e.g. Barber et al., 1998) or with surface based radiometer measurements on the ice (e.g. Mätzler et al., 1984). In this study, the model results are not compared directly to radiometer measurements.

1.3. Sea ice emission modelling

The permittivity (e) of snow is determined by its density and liquid water content (Ulaby et al., 1986). The permittivity of snow is affecting the reflection, transmission and the absorption coefficients. Scattering in the snow pack is detectable for frequencies higher than 10 GHz (Barber et al., 1998) and is important for coarse snow grains or high frequency (?>20 GHz) (Mätzler, 1987). The permittivity of sea ice is largely given by the brine and air-inclusion volume (Shokr, 1998). Important for scattering in sea ice is the size and number density of brine pockets or air bubbles (Winebrenner et al. 1992).

Important radiative processes in a homogeneous snow cover can be described using simple emission models (Ulaby & Stiles, 1980; Mätzler, 1987). However, snow cover on land, ice or sea ice is a layered medium and therefore the simple models fail to simulate observations by not accounting for important reflections between layers (Mätzler et al., 1984; Surdyk & Fily, 1993). Winebrenner et al. (1992) provide a review of different types of emission models that exist for sea ice. The Microwave Emission Model for Layered Snow-packs (MEMLS) is a *"model suitable for simulations of all kinds of physical effects"* (Mätzler et al., 2000, p. 107) and it has been tested and validated for snow-cover on land with satisfactory results. Here MEMLS is extended to include emission from sea ice. The sea ice model and modifications are described in the next section.

2. Extension of MEMLS to sea ice emission

MEMLS, described in Wiesmann & Mätzler (1999), uses the physical snow quantities and structure as input i.e. sequence of layers (*j*), density (*?*), exponential correlation length (p_{ec}), termometric temperature (*T*) and moisture (*W*). In order to apply this model to compute the emission of both snow and sea ice it is necessary to include modules that compute the dielectric properties, and scattering of sea ice. Small liquid brine inclusions also called brine pockets dominate scattering in nilas and first-year ice. In multiyear ice, the voids and air bubbles in the upper ice are the primary scatters (Nghiem et al., 1995). The permittivity of liquid brine is an order of magnitude larger than the permittivity of solid ice and the permittivity of sea ice is therefore primarily a function of brine volume (Ulaby et al., 1986).

The permittivity of sea ice is computed using Polder - Van Santen mixing formulas described in e.g. Shokr (1998). It is a function of pure ice permittivity, inclusion shape and orientation, volume and the brine pockets permittivity (spheres are used because sea ice is assumed isotropic here). These mixing formulas do not account for scattering and therefore the accuracy of the permittivity estimates decreases as a function of frequency. Radiative processes at high frequency are usually confined to the snow cover and it is therefore not expected to be a significant source of error.

MEMLS is valid for snow cover in the range 5-100 GHz. The primary limitation is the estimation of the scattering coefficient using empirical relations, which fit scattering in natural snow cover. For use of MEMLS outside of this frequency range, and for sea ice, it is necessary to compute the scattering coefficient using theoretical relations (Mätzler & Wiesmann, 1999).

The scattering in sea ice is therefore computed using the improved Born approximation (Mätzler, 1998). *"The scattering* [using the improved Born approximation] *increases by a power law of the microwave frequency times the correlation length with a power of approximately 2.5. Above a certain frequency or above a certain correlation length, the increase will saturate in a similar way as Mie scattering does for spheres."* (Mätzler & Wiesmann, 1999; p. 317). It is further noted by Mätzler & Wiesmann that the improved Born approximation fits observations for snow grains which are large compared to the wavelength. It is therefore assumed, in this study, that the improved Born approximation is valid also at high frequency (157 and 183 GHz). Scatters are exclusively air bubbles and voids in multiyear ice and brine pockets in first-year ice. The scattering coefficient is in general a function of the permittivity of pure ice, the permittivity of brine or air, the permittivity of the sea ice mixture, volume of brine or air, microwave frequency and the correlation length of scatters. The exponential correlation length (p_{ec}) is a measure of scatter size and distribution, see e.g. Mätzler (2002).

Natural snow cover consists of both rounded and oblate grains. Re-crystallized snow grains have cup-like forms (Mätzler, 2002). Congelation first-year ice has vertically oriented needle shaped brine pockets while frazil first-year ice has randomly oriented elongated brine pockets (Shokr, 1998). The upper centimetres of first-year ice typically consist of frazil and deeper ice of congelation ice. Frazil layers may also appear at depth (Weeks & Ackley, 1986). In this study both, the snow and sea ice scattering and dielectric properties are assumed isotropic. This assumption significantly simplifies the a priori input to the model and the interpretation of the results, although it is in conflict with the description of the special types of snow and ice above. Anisotropy is a secondary effect that should be included in case specific studies, however, here we are interested in the primary properties affecting the emissivity in a more general description.

These additional modules (sea ice scattering and dielectrics) are hence included in the model computation scheme. The MEMLS code is in MATLAB. With a few minor changes, this sea ice version of MEMLS is now running in GNU Octave (www.octave.org).

3. Sea ice emission modelling experiments using MEMLS

3.1. The sea ice profiles: nilas, first-year and multiyear ice

The constructed profiles of nilas, first-year ice and multiyear ice with typical properties for these ice types are used as input to the model. Table 1-3 presents the input parameters. For all three profiles the skin temperature (synonymous with the upper 1 cm) is -15℃ (258.15 K). The ice/ water interface temperature is -1.8℃ (271.35 K). The temperature profile (1 cm increments) in snow and ice is linear with thermal conductivity in the snow and ice of 0.3 W/mK and 2.1 W/mK respectively. During simulations with liquid water in the snow, the snow temperature is constant -1°C and the snow/ice interface temperature is -5°C. The multiyear ice profile is adapted from Mätzler et al. (1984) and the first-year ice profile is constructed to fit satellite T_b measurements (Tonboe & Andersen, 2004).

Table 1. Nilas profile used as input to MEMLS. The permittivity, *e*, of the sea ice is frequency dependent. Permittivity at frequencies 1.4, 37 and 183GHz cover the range for both the permittivity real part and the loss factor. The permittivity, *e*, at these frequencies by the superscript numbers: 1. *e* at 1.4GHz, 2. *e* at 37GHz and 3. *e* at 183GHz.

No. *j*	Layer depth z_j (m)	Density *?* (kg/m^3)	Exponential correlation length p_{ec} (mm)	Salinity *S* (psu)	Permittivity *e*
1	0.0-0.10	920	0.15	14.0	$3.88+0.07i^1$ $3.55+0.27i^2$ $3.30+0.12i^3$

Table 2. First-year ice profile used as input to MEMLS. The permittivity, *e*, of the sea ice is frequency dependent. Permittivity at frequencies 1.4, 37 and 183GHz cover the range for both the permittivity real part and the loss factor. The permittivity, *e*, at these frequencies by the superscript numbers: 1. *e* at 1.4GHz, 2. *e* at 37GHz and 3. *e* at 183GHz.

No. *j*	Layer depth z_j (m)	Density *?* (kg/m^3)	Exponential correlation length p_{ec} (mm)	Salinity *S* (psu)	Permittivity *e*
1	0.00	260	0.07	0	1.43+0.00i
2	0.07	410	0.10	0	1.76+0.00i
3	0.12	300	0.14	0	1.56+0.00i
4	0.13-1.15	920	0.15	7	$3.62+0.04i^1$ $3.45+0.17i^2$ $3.26+0.09i^3$

Table 3. Multiyear ice profile used as input to MEMLS. The permittivity, *e*, of the sea ice is frequency dependent. Permittivity at frequencies 1.4, 37 and 183GHz cover the range for both the permittivity real part and the loss factor. The permittivity, *e*, at these frequencies by the superscript numbers: 1. *e* at 1.4GHz, 2. *e* at 37GHz and 3. *e* at 183GHz.

No. *j*	Depth z_j (m)	Density *?* (kg/m^3)	Exponential correlation length p_{ec} (mm)	Salinity *S* (psu)	Permittivity *e*
1	0.0	260	0.07	0	1.43+0.00i
2	0.07	450	0.10	0	1.85+0.00i
3	0.08	300	0.10	0	1.52+0.00i
4	0.10	450	0.10	0	1.85+0.00i
5	0.11	300	0.10	0	1.52+0.00i
6	0.16	450	0.10	0	1.85+0.00i
7	0.17	300	0.14	0	1.52+0.00i
8	0.19	750	0.25	0.5	3.20+0.00i^1 3.20+0.01i^2 3.18+0.01i^3
9	0.29-2.49	900	0.20	2.5	3.31+0.01i^1 3.26+0.05i^2 3.21+0.03i^3

3.2. Penetration depth

Assessment of the penetration depth is important when interpreting microwave data, i.e. is the T_b at a certain microwave frequency a result of snow, ice or even deeper ice or water interface radiative processes?

The microwave penetration is strongly reduced in sea ice due to the presence of liquid brine compared to e.g. snow or freshwater ice. The penetration depth, d_p, is defined as (Hallikainen & Winebrenner, 1992),

$$\frac{P(d_p)}{P(0+)} = \frac{1}{e} \qquad (1)$$

where $P(d_p)$ is the transmitted power at depth d_p and $P(0+)$ is the transmitted power just beneath the surface. d_p is a function of the extinction coefficient, i.e. both scattering and absorption, and the transmission loss.

Figures 1-3 show the penetration depth at 50° incidence angle in nilas, first-year and multiyear ice profiles presented in Tables 1-3.

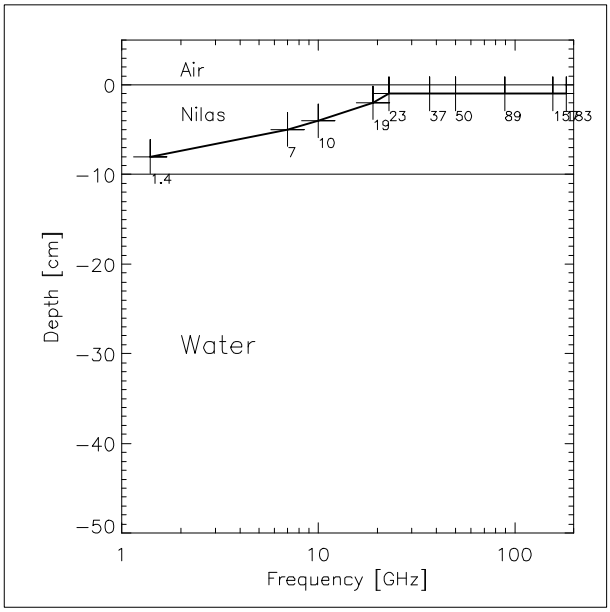

Figure 1. Penetration depth, d_p, at 50° incidence angle in the nilas ice profile described in Table 1, computed at 1.4, 7, 10, 19, 23, 37, 50, 89, 157, and 183 GHz marked with crosses and numbers. The d_p is similar for v and h polarisations.

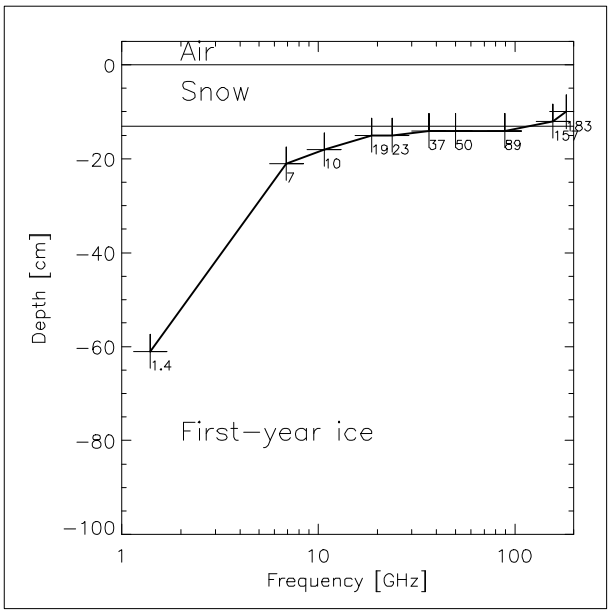

Figure 2. Penetration depth, d_p, at 50° incidence angle in the first-year ice profile described in Table 2, computed at 1.4, 7, 10, 19, 23, 37, 50, 89, 157, and 183 GHz marked with crosses and numbers. The d_p is similar for v and h polarisations.

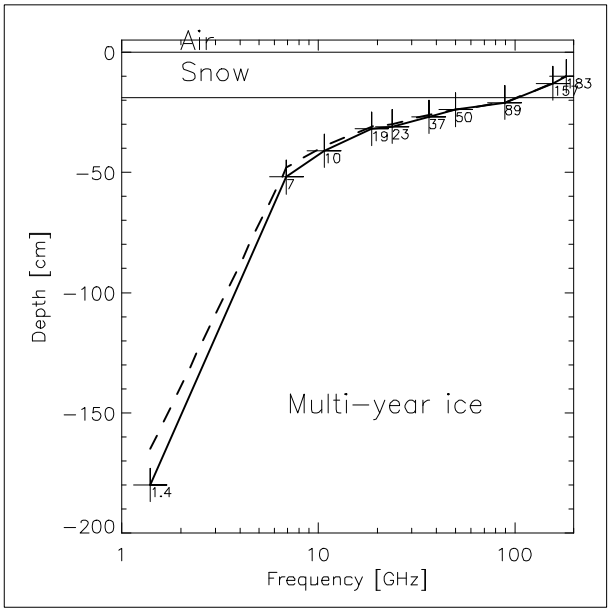

Figure 3. Penetration depth, d_p, at 50° incidence angle in the multiyear ice profile described in Table 3, computed at 1.4, 7, 10, 19, 23, 37, 50, 89, 157, and 183 GHz marked with crosses and numbers. In this particular case, the d_p is different for v (solid line) and h (dashed line) polarisations.

3.3. Depth of icy crust and scattering layer in the first-year ice snow cover

Both scattering and reflections at layers in the snow and ice are processes influencing the brightness temperature at most frequencies. For the natural range of snow grain sizes, scattering is not important at 1.4 GHz. For higher frequency, it is increasingly important to about 89 GHz and for even higher frequency (157 and 183 GHz), scattering tends to saturate for coarse grains. While the influence of grain size and density in unlayered typical sea ice structures has been investigated by Fuhrhop et al. (1997), reflections between layers (snow crusts, air/ snow and snow/ ice interfaces) are also significant for T_b and the polarisation difference (T_v-T_h) at frequencies between 1.4 and 183 GHz, but have not yet been examined in detail. This is the goal of the present study. However, the importance of layering decreases as a function of frequency, due to the shallow penetration and relative significance of scattering even for small scatters at high frequency (89, 157 and 183 GHz).

In the following a model experiment is described where the depth of a 1 cm dense layer (*?* = 500 kg/m^3 crust) and a 1 cm scattering layer (p_{ec} = 0.4 mm re-crystallised snow) is varied in a 13 cm new-snow cover (*?* = 260 kg/m^3, p_{ec} = 0.07 mm) on first-year ice. The experiment illustrates the significance of crust depth as a function of frequency. At 89 GHz (Figure 4), T_v is primarily sensitive to the depth of the scattering layer and T_v-T_h change when the dense layer is at the snow surface or at the snow/ice interface. When the dense layer is at the surface, it increases the air/snow dielectric contrast and T_v-T_h. When the dense layer is at the snow/ice interface, it decreases the ice/snow dielectric contrast and T_v-T_h. The irregular values in Figure 4 along the main diagonal correspond to the overlap between the dense and scattering layers. This part of the diagram is unphysical, hence ignored in the discussion. At frequencies below 89 GHz neither T_v or T_v-T_h are sensitive to the scattering layer depth and T_v is not sensitive to the dense layer depth (not shown here). However, T_v-T_h is sensitive to the dense layer when it is at the surface or above the ice. At frequencies higher than 89 GHz (157 GHz and 183 GHz) T_v is only sensitive to the scattering layer depth. T_v-T_h is sensitive to both the scattering layer and the dense layer at the air/ snow interface. This model experiment indicates that dense layers in the snow pack are most significant when they

modify the large dielectric contrasts in the system, i.e. air/snow- and snow/ice interface, and less important at intermediate depths. The depth of scattering layers is important at frequencies where extinction due to scattering in the background snow pack is significant.

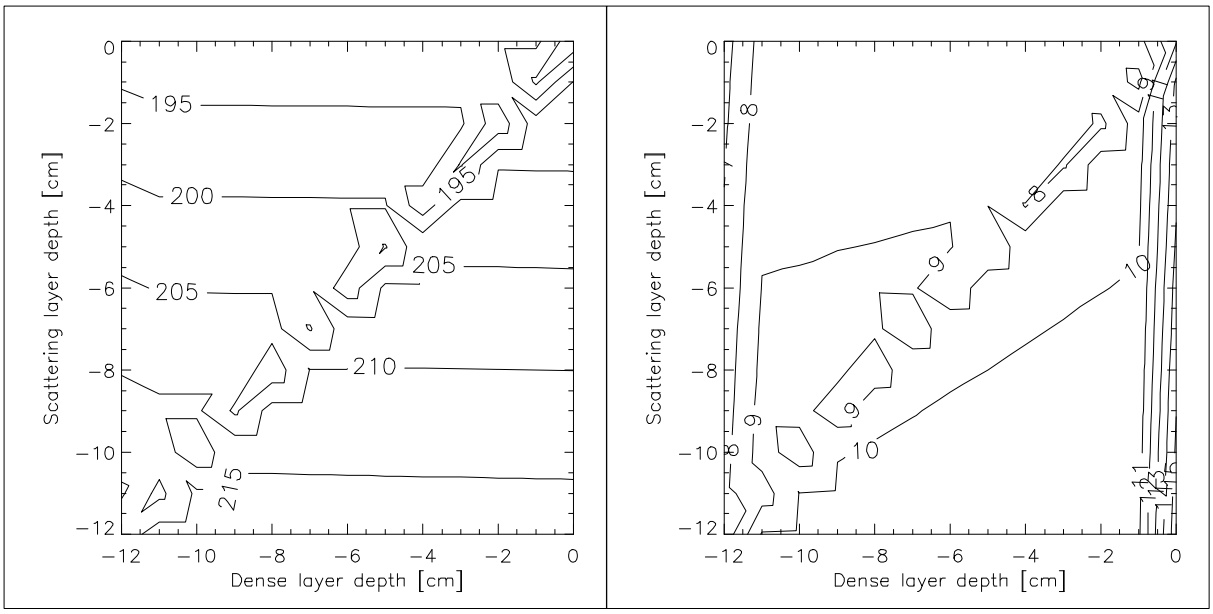

Figure 4. T_v (89 GHz) (left) and T_v-T_h [K] (right) sensitivity to the depth of a dense (*?* = 500 kg/m^3) and scattering layer (p_{ec} = 0.4 mm) of 1 cm thickness in a 13 cm first-year ice snow-pack (*?* = 260 kg/m^3 and p_{ec} = 0.07 mm).

3.4. The T_b and T_v-T_h sensitivity to microphysical parameters of nilas/young ice, first-year ice, and multiyear ice

Meteorological events, such as warm air intruding over the Arctic Ocean sea ice in winter may result in extended metamorphosis of the snow cover. The snow grains grow, grain clusters and crusts are forming and new-snow may accumulate in hours to a few days (Tonboe et al., 2003). These processes in sea ice are not well understood but several properties change simultaneously. Changing just one parameter at a time as we do in the following model sensitivity study is therefore not realistic. However, it is instructive to see the significance of each single parameter. Each parameter listed in Table 4 is varied between the given ranges while other input parameters are constant as presented in Tables 1-3. These examples illustrate the significance of scattering and reflections between layers at different levels in the snow-ice system.

Table 4. The parameters, which are varied in sensitivity studies.

Ice type	Parameter	Depth [cm]	Range
Nilas/young ice	Salinity	ice column	2.5-18 psu
	Ice thickness	ice column	3-31.5 cm
First-year ice	Upper snow density	0-7	260-450 kg/m^3
	Mid snow density	7-12	260-450 kg/m^3
	Bottom snow p_{ec}	12-13	0.07-0.45 mm
	Upper ice salinity	13-19	2.5-18 psu
	Snow liquid water	snow column	0-14 %
	Snow thickness	snow column	1.5-31.5 cm
Multiyear ice	Upper snow density	0-4	260-450 kg/m^3
	Mid snow density	4-7	260-450 kg/m^3
	Bottom snow p_{ec}	17-19	0.07-0.45 mm
	Upper ice density	19-29	750-900 kg/m^3
	Snow liquid water	snow column	0-14 %
	Snow thickness	snow column	1.5-31.5 cm

The importance of the different snow and ice parameters for the T_v and T_v-T_h are categorised in Table 5. Variations in T_v larger than 5 K belong to category 1, others to category 2. Variations in T_v-T_h larger than 10 K are category 1.

Table 5. The importance of the different snow and ice parameters for the T_v and T_v-T_h. Category 1 is for *?*T_v>5 K and *?*(T_v-T_h)>10 K. Others belong to category 2.

First-year ice			Multiyear ice		
	T_v	T_v-T_h		T_v	T_v-T_h
Snow thickness	**2**	1.4-50GHz: **2** 89-183GHz: **1**	Snow thickness	157, 183GHz: **1** Others: **2**	7, 89GHz: **1** Others: **2**
Vol. liquid water	7-19GHz:**1** Others: **2**	7-183GHz: **1** 1.4GHz: **2**	Vol. liquid water	7-183GHz: **1** 1.4GHz: **2**	7GHz: **1** Others:**2**
Upper snow layer ?	**2**	1.4-7GHz: **2** 10-183GHz: **1**	Upper snow layer ?	1.4, 37-183GHz: **1**	7-183GHz: **1** 1.4GHz: **2**
Mid snow layer ?	**2**	**2**	Mid snow layer ?	1.4, 50-183GHz: **2**	7-183GHz: **1** 1.4GHz: **2**
Bottom snow layer p_{ec}	=50: **1** Others: **2**	**2**	Bottom snow layer p_{ec}	89GHz: **1** Others: **2**	**1**
Upper ice salinity	10-89GHz: **1** 1.4, 7, 157, 183GHz: **2**	**2**	Upper ice ?	**2**	**2**

The first-year ice T_v variability is in general low. It is below 10 K except for bottom snow layer correlation length at 89, 157 and 183 GHz, T_v decrease, i.e. the high frequency T_v is affected by scattering. The first-year ice T_v-T_h is particularly sensitive to volumetric liquid water at 7-50 GHz and upper snow layer density at 10-183 GHz.

Changing just one parameter gives results, which are interpreted relatively easily while two or more parameters create complicated but more realistic scenarios. Therefore, we test the following

parameter pairs. Nilas: Salinity and thickness. First-year ice: Upper snow density and bottom snow correlation length, mid snow density and upper ice salinity, snow liquid water and snow thickness. Multiyear ice: Upper snow density and bottom snow correlation length, mid snow density and upper ice density, snow liquid water and snow thickness.

The results for the nilas/ young ice parameter-pair show that the ice thickness only influences T_v and T_v-T_h at frequency = 19 GHz. At 1.4 GHz and 7 GHz, T_v and T_v-T_h are sensitive throughout the complete range of salinities. At 10 GHz and 19 GHz T_v and T_v-T_h are only sensitive to thickness at low salinity (Table 4). Further, that T_v-T_h is moderately sensitive (2-7 K) to salinity at all frequencies. T_v-T_h (19 GHz) is the most sensitive while *?* = 50 GHz are least sensitive. T_v is sensitive to salinity = 19 GHz.

The liquid water content of the snow layer and the snow thickness is an important parameter combination for first-year ice at 7 to 89 GHz (most significant at low frequency). Figure 5 show T_v-T_h (89 GHz). The snow thickness plays a role for T_v-T_h until the water content in the snow reach about 1 % by volume. At that point, the attenuation in the snow is considerable and the surface reflectivity dominate the radiative processes and T_v-T_h increase as a function of permittivity.

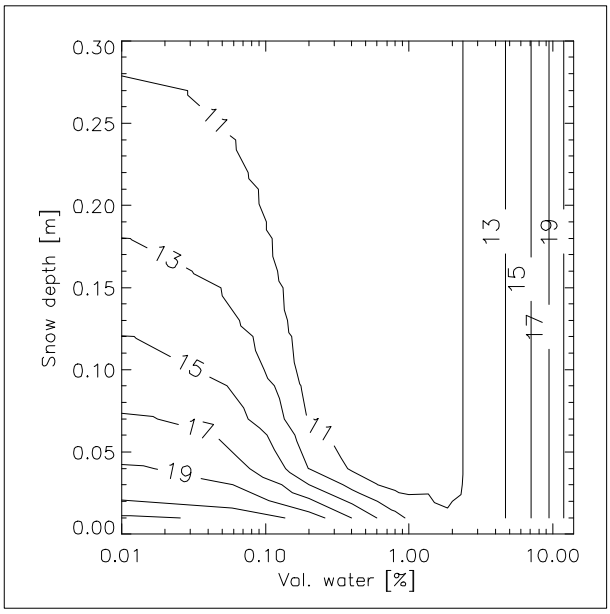

Figure 5. T_v-T_h (89 GHz) [K] sensitivity to first-year ice snow depth (1.5-30 cm) and volumetric liquid water content in the snow (0-14 %).

4. Parameterisation of sea ice emissivity for atmospheric retreival

The assimilation of atmospheric parameters derived from microwave satellite data e.g. AMSU has a significant impact on both global (ECWMF) and regional (HIRLAM) weather prediction models (Prigent et al., 2004). The principle is to separate the atmospheric emissivity from the surface emissivity in the T_b measurements from space, thus the atmospheric part is parameterised in terms of temperature or water vapour. The surface emissivity, which is high for sea ice compared to open water, can be determined at frequencies where the atmosphere is largely transparent in the 'atmospheric windows'. This allows referring the emissivities at the sounding frequencies to those at the window frequencies by interpolation using emission models. Temperature sounding uses frequencies around 50 GHz and humidity sounding uses frequency = 85 GHz. Surface emissivity estimation at sounding frequencies will become even more important with SSM/IS because it combines observations at the window and at the sounding frequencies on one sensor observing at all frequencies with a constant incidence angle.

Figure 6 shows the simulated correlation between first- and multiyear ice T_v at the 10 microwave frequencies (1.4-183 GHz) using all parameter pairs described in the previous section. The many off-diagonal points at the 37/50 GHz (Figure 6f), 50/89 GHz (Figure 6g) and 89/157 GHz (Figure 6h) plots indicate that simple linear models are inadequate to relate T_b at window frequencies to sounding frequencies.

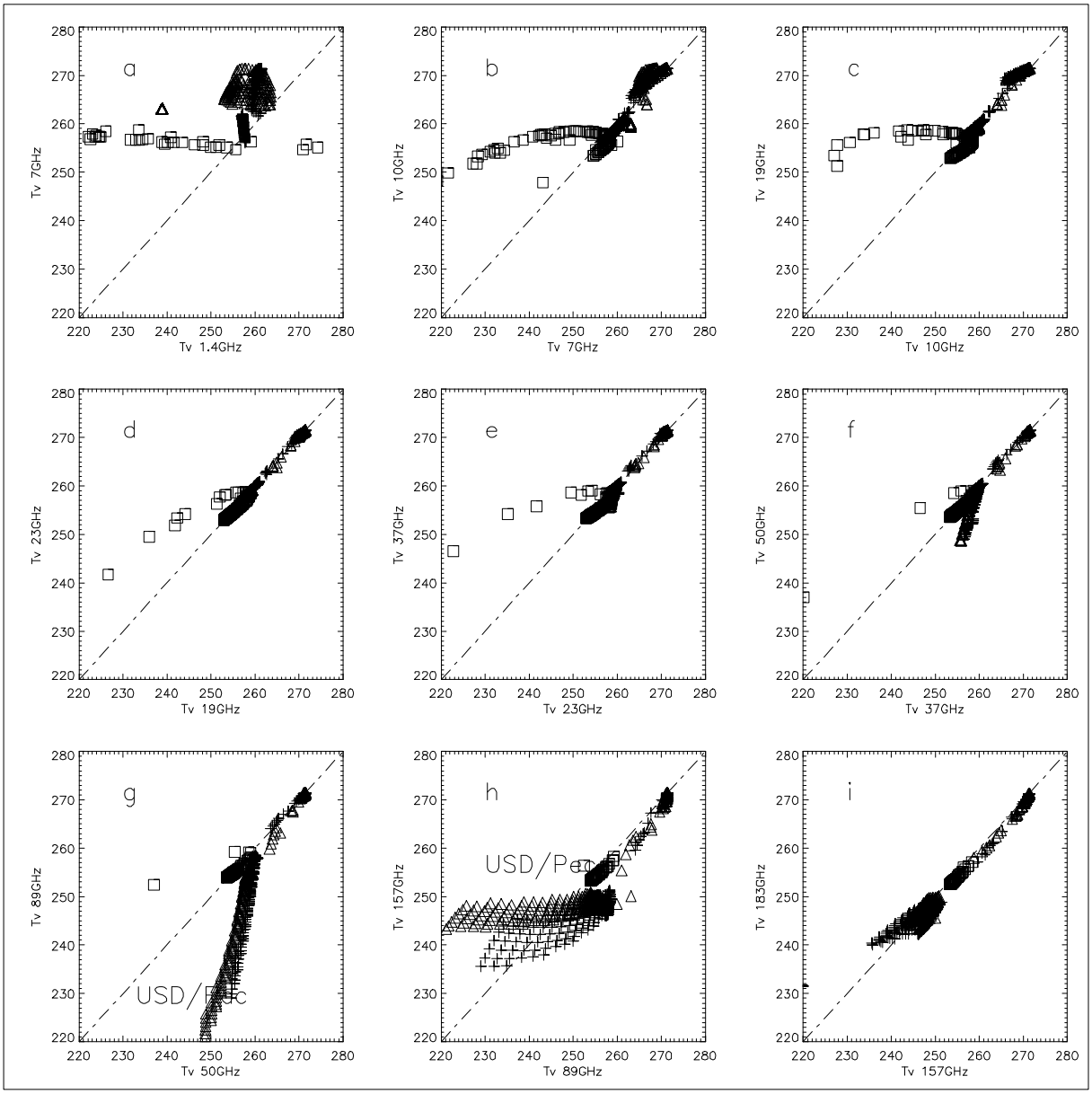

Figure 6a-i. The simulated correlation between nilas (?), first-year ice (+), and multiyear ice (?) T_v for the 10 frequencies using all parameter pairs in Table 4 (every 3rd data point). The off-diagonal points marked by USD/p_{ec} in 6g and 6h are associated with the upper snow density (USD)/ bottom snow layer correlation length (p_{ec}) parameter pair. The nilas T_v extend beyond the range of 6a-6e.

The nilas T_v is lower at the lowest of the two frequencies in each of Figure 6a-6e (frequency = 37GHz). The nilas points follow a line-like cluster about 45° to the diagonal. For higher frequency, the nilas points are close to the diagonal. The snow thickness/ snow liquid water parameter pair T_v points are close to the diagonal except in Figure 6h where T_v (157 GHz) is lower than T_v (89 GHz). In Figures 6f - 6i the off-diagonal points are associated with the upper snow density/ bottom snow layer correlation length parameter pair for both first-year and multiyear ice. This is the most important parameter combination among the pairs in Table 4 for the first-year and multiyear ice T_v sensitivity at medium and high frequency. The T_v variability is similar when varying more than two parameters simultaneously, e.g. first-year ice upper and mid snow density, bottom snow correlation length and salinity (not shown).

5. The sea ice concentration estimate surface emissivity sensitivity

Current ice concentration algorithms use satellite microwave T_b between 6 and 89 GHz as input. The mean accuracies of some of the more common algorithms, used for SSM/I data, such as NASA Team (Cavalieri et al., 1984) and Bootstrap (Comiso, 1986) are reported to be 1-6 % in winter (Steffen & Schweiger, 1991; Emery et al., 1994; Belchansky & Douglas, 2002). At high ice concentrations, even small changes in the sea ice concentration have a significant impact on energy fluxes between the ocean and the atmosphere. Therefore, ice concentration is an important ice cover parameter to estimate accurately (Steffen & Schweiger, 1991).

The computed ice concentration accuracy is further degraded by particular atmospheric constituents like cloud liquid water, where NASA Team ice concentration erroneously can increase by about 10 % (Oelke, 1997). Changes in the surface emissivity can depress the computed ice concentration by 20 % (Tonboe et al., 2003). Toudal (1994) argued that variations in surface emissivity is a very important error source in sea ice concentration retrievals over consolidated ice from satellite passive microwave measurements.

The sensitivity of the different ice concentration algorithms e.g. NASA Team, Bootstrap and Near 90 GHz (Svendsen et al., 1987) to the atmosphere or surface brightness temperature is different as shown in Figure 6 for a case in Baffin Bay. Coincident SAR images show that the real ice concentration in this area is stable above 94 % (Tonboe et al., 2003).

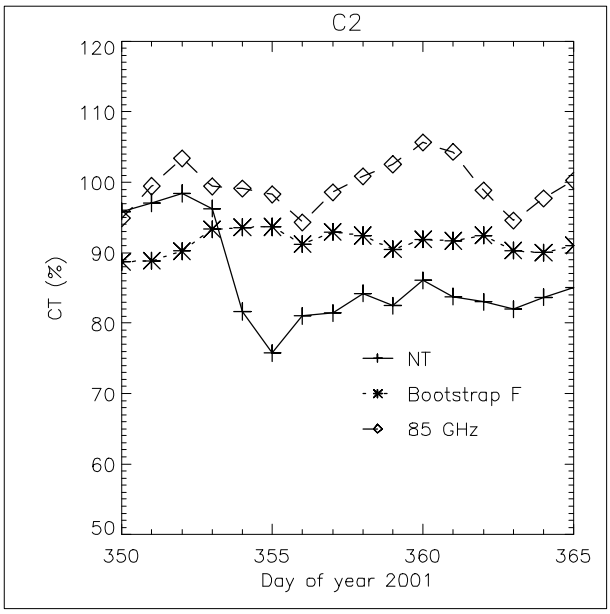

Figure 6. The computed ice concentration in a small area in Baffin Bay (62.6°W, 71.5°N) using NASA Team, Bootstrap and Near 90GHz algorithms, December 2001. The measured air temperature on a nearby meteorological station on the Greenland coast (Upernavik) increase above 0°C on day of year 353/354 and the freeze-up begin on day 357 (from Tonboe et al., 2003).

The sea ice emissivity normally changes during winter because of ice growth, snowfall, diurnal cycling and snow/ice metamorphosis. Warm air outbreaks (Figure 6) over the consolidated sea ice pack in Baffin Bay and Fram Strait/ Arctic Ocean during winter is a possibility to investigate the sensitivity of the ice concentration estimate to changes in the snow and ice cover emissivity in the course of days (Tonboe et al., 2003). While the actual ice concentrations remain close to 100 %

during and after the advection of warm air followed by snowfall and possibly rain, the formation of depth hoar and icy layers in the snow pack and in general the metamorphism accelerates as described in e.g. Drinkwater et al. (1995) and Garrity (1992). These winter warm air events may influence large areas (about 360 000 km^2) and on a weekly timescale smaller areas (15 000 km^2) along the ice edge (Tonboe et al., 2003).

The algorithms sensitivity to surface emissivity and thermometric temperature of the target depend on the selected polarisations and frequencies (Comiso et al., 1997; Emery et al., 1994; Toudal, 1994). Emission models can be used to analyse and compute the sensitivity of the retrieved ice concentration to the microphysical properties of the snow and ice and to select and develop algorithms with low sensitivity to variations in the surface emissivity. Figure 7 shows the modelled sensitivity of the NASA Team ice concentration to the density of the upper snow layer and correlation length of the bottom 1 cm snow layer.

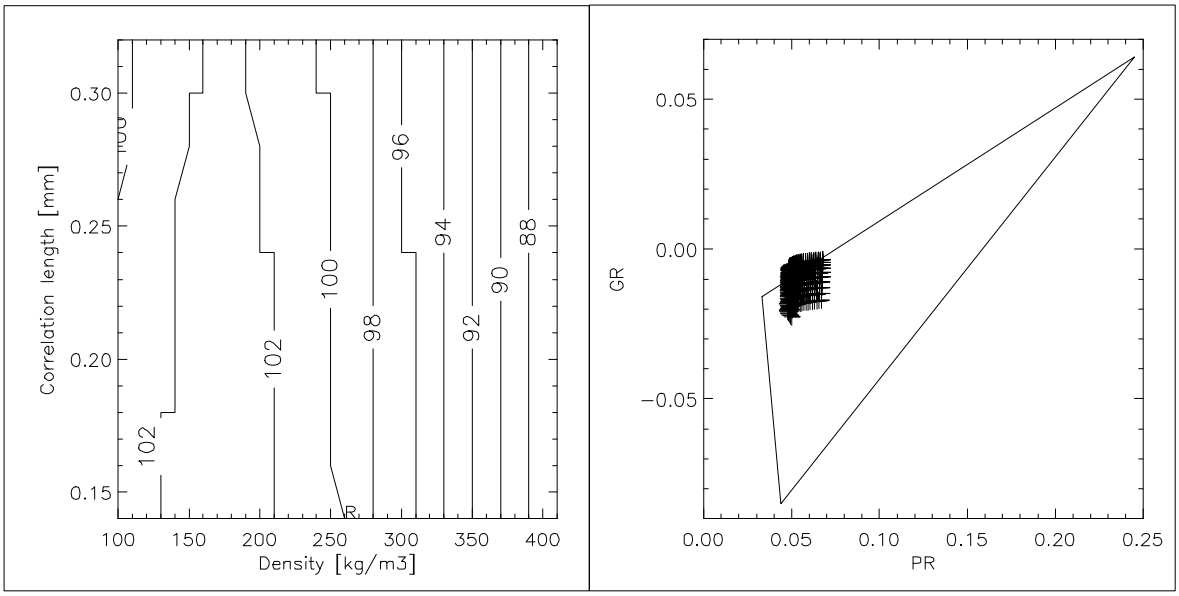

Figure 7. Sensitivity of the NASA Team algorithm sensitivity to variations in layering and grain size in the snow cover on first-year ice (left). Simulated data placed in the PR_{19} and $GR_{19v/37v}$ space with the approximate NASA Team retrieval triangle in the background (right). Tie-points based on Andersen (1999) (from Tonboe & Andersen, 2004).

The changes are persistent but recover in the course of months, e.g. the NASA Team ice concentration estimate is sensitive to layering in the snow pack and in particular to the air/ snow dielectric contrast (i.e. density of the snow surface). Surface crusts with relatively high permittivity form during temporary warming (this strongly affects the NASA Team ice concentration), however new snow on top of the crust will decrease the dielectric contrast again thus reducing its influence on the brightness temperature (see section 3.3). The NASA Team total ice concentration is robust to the simulated variations in the bottom snow layer correlation length.

Tonboe & Andersen (2004) made a model sensitivity study using MEMLS of nine common ice concentration algorithms where both the upper snow density and the bottom snow correlation length of a first-year ice profile (Table 2) were varied as described in Table 4. The model simulations showed:

1) the combination of T_v (19 GHz) and T_v (37 GHz) as used in the Comiso Bootstrap algorithm in frequency mode, in the NORSEX (Svendsen et al., 1983) and in the Cal-val (Ramseier, 1991) algorithms has low sensitivity to the simulated emissivity changes,

2) algorithms also using T_h like Bristol (Smith, 1996), NASA Team and Bootstrap in polarisation mode are sensitive to the simulated density of the upper snow layer.

They further found that the simulated high sensitivity of the 89 GHz polarisation difference (T_v-T_h) to both density and the correlation length makes the algorithms using the high frequency channel like Near 90 GHz and TUD (Pedersen, 1998) very sensitive to the simulated snow cover emissivity.

Mätzler et al. (1984) reported results from a field experiment that the high frequency (94 GHz) polarisation difference appeared insensitive to ice lenses at 7 cm depth in the snow. This observation was explained by strong attenuation and isotropic scattering in the upper snow layer. They further noted that *"… at 94 GHz the surface reflectivity will lead primarily to polarization effects …"* (Mätzler et al., 1984, p. 335). The shallow penetration of the near 90GHz microwaves (confined to the upper centimetres of the snow cover) means that different ice types with snow cover has similar radiative signatures. Furthermore, ice lenses below the upper centimetres of snow are only vaguely affecting the near 90 GHz emissivity. In other words, the near 90 GHz emissivity is largely insensitive to ice type and ice layers within the snow-pack, which are affecting and complicating the interpretation of emissivity at e.g. 19 and 37 GHz. These observations lead to the development of the Near 90 GHz ice concentration algorithm that exploits the higher spatial resolution at this frequency (Svendsen et al., 1987; Pedersen, 1998; Kaleschke et al., 2001).

However, the near 90 GHz polarisation difference is indeed sensitive to snow-ice surface emissivity. The model experiment indicate that the polarisation difference (at 89 GHz) increase as a function of air-snow dielectric contrast/ reflectivity (upper snow layer density). The air-snow density contrast was not explicitly the theme of the laboratory experiment of Barber et al. (1998). Even so, they note that as the snow cover permittivity increases: 1) e_h (90 GHz) decreases, 2) e_v is stable. This confirms our model experiments.

6. New sensors: L-band sea ice radiometry with SMOS

Before the launch of the European Soil Moisture and Ocean Salinity mission (SMOS) in 2007 it is largely unknown what the benefit of L-band (1.4GHz) radiometer measurements will be for sea ice mapping. The SMOS mission is described in Kerr et al. (2001). L-band radiometer measurements have been acquired over sea ice only during summer in order to investigate the influence of melt ponds (melt pond 2000, US campaign, Klein et al., 2004). Models need to be used to investigate the winter sea ice mapping potential for L-band radiometers. The primary limitation to the valid frequency range in MEMLS is the estimation of scattering. MEMLS is expected to be valid at L-band since scattering at this frequency is insignificant.

We notice that L-band penetrate to near the ice/ water interface in nilas (Figure 1). To investigate this further Figure 8 shows the evolution of the emissivity at 1.4 GHz and 7 GHz for a growing new- young ice sheet (3-31 cm) without snow cover. It seems that the 1.4 GHz emissivity is affected by the water emissivity throughout the range of thickness while at 7 GHz the emissivity relatively quickly rises from typical water to ice emissivities and reaches saturation at about 20 cm thickness.

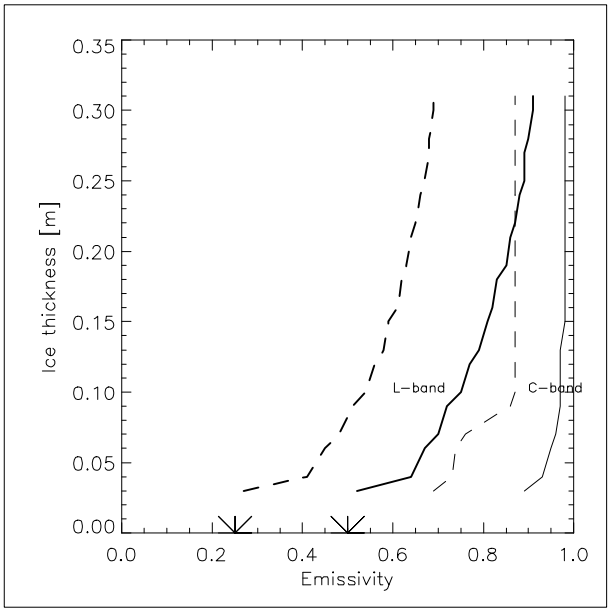

Figure 8. 1.4 GHz (L-band) and 7 GHz (C-band) emissivity from a growing ice sheet (3-31cm) without snow cover. e_v (full line) and e_h (dashed line). The water emissivity is assumed similar at the two frequencies: e_v = 0.50 and e_h = 0.25, marked by arrowheads on the x-axis.

Sea ice salinity increases with the growth rate (Weeks & Ackley, 1986) which in turn decreases with thickness because the ice layer insulates and reduces cooling of the ice/ water interface. Hence, as ice grows from the initial thin nilas (3 cm) to thick young ice (30 cm) it experiences a decrease in total salinity. In addition, the brine volume (i.e. the permittivity) in the upper ice decreases as a function of ice thickness and the resulting reduction in upper ice temperature. Figure 9 shows T_v (1.4 GHz) as a function of the total thickness and of the salinity of a thin ice sheet. Thin saline ice T_v (1.4 GHz) and thick less saline ice T_v are similar. Also, T_v-T_h (1.4 GHz) is ambiguous with respect to salinity and thickness. Mapping of thin ice thickness using L-band is therefore difficult.

In any case, formation of thin ice (nilas) on the scale of the SMOS resolution (50 km) is rare and in most cases, new ice areas are mixed with older ice (young-, first- and multiyear ice) and open water.

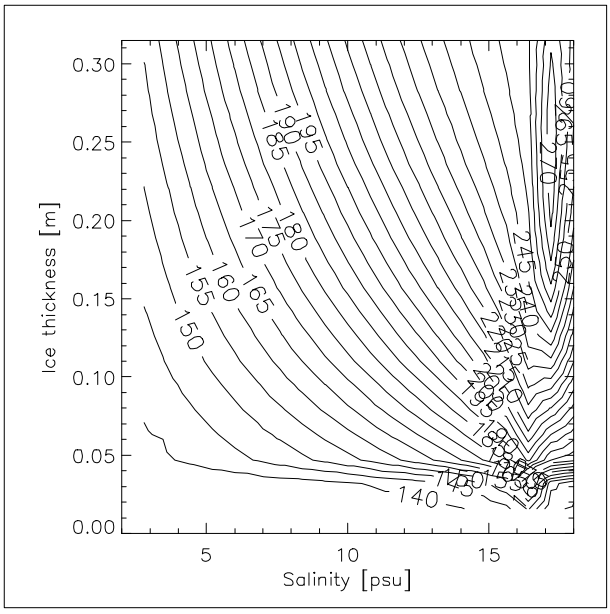

Figure 9. T_v (1.4GHz) sensitivity to ice thickness (3-31.5 cm) and salinity (2.5-18 psu) in nilas/ young ice.

The 1.4GHz T_v (Figure 6a) is obviously influenced by other parameters than T_v at other frequencies. In Figure 6a no line like dependencies are observed indicating that none of the varied parameters has a predominant influence.

7. Conclusions

MEMLS has been set up for sea ice and the usefulness of sea ice emission modelling demonstrated with three different applications, i.e. surface emissivity and atmospheric parameterisation, sensitivity of the ice concentration estimate to the variable emissivity and future sensors. The specific conclusions are:

- The penetration depth at 157 and 183 GHz in first- and multiyear ice is confined to the snow layer, 89 GHz penetrate to the ice surface. Penetration depth is considerable at 1.4 GHz with 60 cm depth in first-year and 180 cm in multiyear ice. On the one hand, frequencies higher than 19 GHz only penetrate the nilas surface. On the other hand, radiation at 1.4 GHz penetrates to near the nilas/ water interface.
- The position of icy crusts in the snow layer influences brightness temperature when the large dielectric contrasts of the system are modified by the crust, i.e. if the crust is near the air/snow or near the snow/ice interface. The scattering layer depth is significant at high frequency (89, 157 and 183 GHz).
- Scattering and reflections at layers are the radiative processes affecting the brightness temperature. These processes occur at many levels in the snow ice system. Environmental processes that accelerate the change of scattering and reflection parameters in the snow are e.g. temporary warming. During actual melt, liquid water in the snow is significant and increases T_v up to 10 K for about 1 % liquid water content.
- Simple emission models to interpolate between window and sounding frequencies are needed to separate surface and atmospheric contribution to radiation measured at the satellite emission for atmospheric parameterisation. Since scattering is in the snow is important at sounding frequencies, an adequate scattering description in the model seems to be paramount for obtaining the correct level of T_v or e_v.
- MEMLS has successfully been used in the pursuit of ice concentration algorithms with low sensitivity to surface emissivity. In the case, presented, T_v combinations at 19 and 37 GHz seemed to be most robust.
- 1.4 GHz brightness temperature is sensitive to both thin ice thickness and salinity. The ambiguity is not lifted by T_v-T_h.

8. Open challenges

Sea ice emission modelling is still young compared to modelling of land and ocean. Several issues remain:

One of the most important problems remaining for sea ice emission modellers is to develop computationally fast and relatively simple emissivity models for sea ice to estimate the surface emissivity from window to sounding frequencies. This is required for atmospheric parameterisation (temperature and water vapour) and the results are significant for assimilation of microwave radiometer data into weather prediction models operating globally or regionally at high latitudes.

Snow mapping on sea ice is an important issue not only for the parameterization of fluxes but also for other microwave remote sensing applications. As shown earlier, the snow cover on first-year ice has a significant impact on e.g. the radiometer ice concentration estimate. Models for snow parameterisation using inversion techniques must be relatively simple and rely only on the most important snow parameters (e.g. Hewison & English, 1999). The development of such models could take departure in all-round complex models like MEMLS to arrive at models such as 'the HUT snow microwave emission model' (Pulliainen et al., 1999), successfully used for model inversion for land snow cover parameterisation. Toudal (1994) demonstrated earlier how forward models of ice emissivity could be used in inversion algorithms. Results from MEMLS will provide a very important step towards such forward models.

Mätzler et al. (2000) describe a coupled physical and emissivity snow model that successfully simulate the effects of snow depth on microwave parameters. Physical sea ice models coupled to emission models similar to the approach of Mätzler et al. would make it possible to seek brightness temperature combinations, which are unlikely influenced by ice emissivity for use in ice concentration algorithms. Realistic description of sea ice metamorphosis and the snow and ice profile is a necessary prerequisite for reliable model results. Both models should further treat the physics of saline snow.

Validation of sea ice emission models is the overriding issue in all of the above future applications. Future model developments should include a substantial validation component. Logistics is a larger problem on sea ice than on land and conditions are not as homogeneous as in the ocean but validation is anyway the key to the above sea ice applications.

9. References

Barber, D. G., A. K. Fung, T. C. Grenfell, S. V. Nghiem, R. G. Onstott, V. I. Lytle, D. K. Perovich, & A. J. Gow (1998). The role of snow on microwave emission and scattering over first-year sea ice. *IEEE Transactions on Geoscience and Remote Sensing 36*(5), 1750-1763.

Barber, D. G., S. P. Reddan, & E. F. LeDrew (1995). Statistical characterisation of the geophysical and electrical properties of snow on landfast first-year sea ice. *Journal of Geophysical Research 100*(C2), 2673-2686.

Belchansky, G. I., & D. C. Douglas (2002). Seasonal comparisons of sea ice concentration estimates derived from SSM/I, OKEAN, and RADARSAT data. *Remote Sensing of Environment 81*, 67-81.

Carsey, F. D., R. G. Barry, D. A. Rothrock, & W. F. Weeks (1992). Status and future directions for sea ice remote sensing. In: F. D. Carsey (Ed.). *Microwave remote sensing of sea ice, Geophysical monograph 68* (pp. 444-446). Washington DC: American Geophysical Union.

Cavalieri, D.J, P. Gloersen, & W. J. Cambell (1984). Determination of sea ice parameters with the NIMBUS 7 SMMR. *Journal of Geophysical Research 89*(D4), 5355-5369.

Comiso, J.C. (1986). Characteristics of arctic winter sea ice from satellite multispectral microwave observations. *Journal of Geophysical Research 91*(C1), 975-994.

Comiso, J.C., D. J. Cavalieri, C. L. Parkinson, & P. Gloersen (1997). Passive microwave algorithms for sea ice concentration: a comparison of two techniques. *Remote Sensing of Environment 60*, 357-384.

Drinkwater, M. R., R. Hosseinmostafa, & P. Gogineni (1995). C-band backscatter measurements of winter sea ice in the Weddell Sea, Antarctica. *International Journal of Remote Sensing 16*(17), 3365-3389.

Emery, W. J., C. Fowler, & J. Maslanik (1994). Arctic sea ice concentrations from special sensor microwave imager and advanced very high resolution radiometer satellite data. *Journal of Geophysical Research 99*(C9), 18329-18342.

Eppler, D. T. and 14 others (1992). Passive microwave signatures of sea ice. In: F. D. Carsey (Ed.). *Microwave remote sensing of sea ice, Geophysical monograph 68* (pp. 47-71). Washington DC: American Geophysical Union.

Fuhrhop, R., C. Simmer, M. Schrader, G. Heygster, K.-P. Johnsen, & P. Schüssel (1997). Study of passive remote sensing of the atmosphere and surface ice. Berichte aus dem Institut für Meereskunde an der Christian-Albrechts Universität, Kiel 297, p. 241.

Garrity, C. (1992). Characterisation of snow on floating ice and case studies of brightness temperature changes during the onset of melt. In: F. D. Carsey (Ed.). *Microwave remote sensing of sea ice, Geophysical monograph 68* (pp. 313-328). Washington DC: American Geophysical Union.

Gogineni, S. P., R. K. Moore, T. C. Grenfell, D. G. Barber, S. Digby, & M. Drinkwater (1992). The effects of freeze-up and melt processes on microwave signatures. In: F. D. Carsey (Ed.). *Microwave remote sensing of sea ice, Geophysical monograph 68* (pp. 329-341). Washington DC: American Geophysical Union.

Hewison, T. J. & S. J. English (1999). Airborne retrivals of snow and ice surface emissivity at millimeter wavelengths. *IEEE Transactions on Geoscience and Remote Sensing 37*(4), 1871-1879.

Kaleschke, L., C. Lüpkes, T. Vihma, J. Haarpaintner, A. Bochert, J. Hartmann & G. Heygster (2001). Sea Ice Remote Sensing for Mesoscale Ocean-Atmosphere Interaction Analysis. *Canadian Journal of Remote Sensing 27*(5), 526-537.

Kerr, Y. H., P. Waldteufel, J.-P. Wigneron, J.-M. Martinuzzi, J. Font & M. Berger (2001). Soil moisture retrieval from space: the soil moisture and ocean salinity (SMOS) mission. *IEEE Transactions on Geoscience and Remote Sensing 39*(8), 1729-1735.

Klein, M., A. J. Gasiewski, D. J. Cavalieri, & T. Markus (2004). Meltpond2000 Polarimetric Scanning Radiometer Sea Ice Brightness Temperatures. Boulder, CO, USA: National Snow and Ice Data Center. Digital media.

Mätzler, C. & A. Wiesmann (1999). Extension of the microwave emission model of layered snowpacks to coarse grained snow. *Remote Sensing of Environment 70*, 317-325.

Mätzler, C. (1987). Applications of the interaction of microwaves with the natural snow cover. *Remote Sensing Reviews 2*(2), 259-391.

Mätzler, C. (2002). Relation between grain-size and correlation length of snow. *Journal of Glaciology 48*(162), 461-466.

Mätzler, C., R. O. Ramseier, & E. Svendsen (1984). Polarisation effects in sea ice signatures. *IEEE Journal of Oceanic Engineering OE-9*(5), 333-338.

Mätzler, C. A. Wiesmann, J. Pulliainen & M. Hallikainen (2000). Development of microwave emission models of snowpacks. In: C. Mätzler (Ed.). *Radiative transfer models for microwave radiometry*. European Commission COST Action 712, final report (pp. 105-116).

Nghiem, S. V., R. Kwok, S. H. Yueh, & M. R. Drinkwater (1995). Polarimetric signatures of sea ice – 1. Theoretical model. *Journal of Geophysical Research 100*(C7), 13665-13679.

Oelke, C. (1997). Atmospheric signatures in sea ice concentration estimates from passive microwaves: modelled and observed. *International Journal of Remote Sensing 18*(5), 1113-1136.

Parkinson, C. L. & D. J. Cavalieri (1989). Arctic sea ice 1973-1987: seasonal, regional, and interannual variability. Journal of Geophysical Research 94(C10), 14499-14523.

Pedersen, L.T. (1998). Chapter 6.2 in Sandven et al. *IMSI report no. 8. Development of new satellite ice data products*. Bergen, Norway: NERSC Technical Report no. 145, Nansen Environmental and Remote Sensing Center

Prigent, C., F. Chevallier, F. Karbou, P. Bauer, G. Kelly (2004). AMSU-A land surface emissivity estimation for numerical weather prediction. NWP SAF, document no. NWPSAF-EC-TR-009, EUMETSAT.

Pulliainen, J. T., J. Grandell, & M. T. Hallikainen (1999). HUT snow emission model and its applicability to snow water equivalent retrieval. *IEEE Transactions on Geoscience and Remote Sensing 37*(3), 1378-1390.

Ramseier R.O. (1991) Sea ice validation. In J.P. Hollinger (ed.), *DMSP special sensor microwave/imager calibration/validation - Final report volume II*, Washington, DC: Naval Research Laboratory

Selbach, N. (2003). Determination of total water vapour and surface emissivity of sea ice at 89GHz, 157GHz and 183GHz in the Arctic winter. Ph.D. Thesis, *Berichte aus dem Institut für Umweltphysik.* Berlin:Logos-Verlag, Vol. 21, p. 191.

Shokr, M. E. (1998). Field Observations and model calculations of dielectric properties of Arctic sea ice in the microwave C-band. *IEEE transactions on Geoscience and Remote Sensing 36*(2), 463-478.

Smith, D.M. (1996) Extraction of winter sea ice concentration in the Greenland and Barents Seas from SSM/I data. *International Journal of Remote Sensing 17*(13), 2625-2646.

Steffen, K., & A. Schweiger (1991). NASA Team algorithm for sea ice concentration retrieval from Defence Meteorological Satellite Program Special Sensor Microwave Imager: comparison with Landsat satellite imagery. *Journal of Geophysical Research 96*(C12), 21971-21987.

Surdyk, S. & M. Fily (1993). Comparison of the passive microwave spectral signature of the Antarctic ice sheet with ground traverse data. Annals of Glaciology 17, 161-166.

Svendsen, E., K. Kloster, B. Farelly, O. M. Johannesen, J. A. Johannesen, W. J. Campbell, P. Gloersen, D. J. Cavalieri & C. Mätzler (1983) Norwegian remote sensing experiment: Evaluation of the Nimbus 7 scanning multichannel microwave radiometer for sea ice research. *Journal of Geophysical Research 88*(C5), 2781-2791

Tonboe, R. T., & S. Andersen (2004). Modelled radiometer algorithm ice concentration sensitivity to variations of the Arctic sea ice snow cover. *Danish Meteorological Institute Scientific Report 04-03*, p. 34.

Tonboe, R. T., S. Andersen & L. Toudal (2003). Anomalous winter sea ice backscatter and brightness temperatures. *Danish Meteorological Institute Scientific Report 03-13*, p. 59.

Toudal, L. (1994). Merging microwave radiometer data and meteorological data for improved sea ice concentrations. *EARSeL Advances in Remote Sensing 3*(2) XII, 81-89.

Tucker, W. B., T. C. Grenfeld, R. G. Onstott, D. K. Perovich, A. J. Gow, R. A. Shuchman & L. Sutherland (1991). Microwave and physical properties of sea ice in the winter marginal ice zone. *Journal of Geophysical Research 96*(C3), 4573-4587.

Ulaby, F. T., & W. H. Stilles (1980). The active and passive microwave response to snow parameters 2. water equivalent of dry snow. *Journal of Geophysical Research 85*(C2), 1045-1049.

Ulaby, F. T., R. K. Moore & A. K. Fung (1986). *Microwave Remote Sensing, From Theory to Applications, vol. 3*. Dedham MA: Artech House.

Weeks, W. F., & S. F. Ackley (1986). The growth, structure and properties of sea ice. In N. Untersteiner (Ed.), *The geophysics of sea ice*. (pp. 9-164). New York: Plenum.

Wiesmann, A. & C. Mätzler (1999). Microwave emission model of layered snowpacks. *Remote Sensing of Environment 70*, 307-316.

Winebrenner, D. P., J. Bredow, A. K. Fung, M. R. Drinkwater, S. Nghiem, A. J. Gow, D. K. Perowich, T. C. Grenfell, H. C. Han, J. A. Kong, J. K. Lee, S. Mudaliar, R. G. Onstott, L. Tsang, R. D. West (1992). Microwave sea ice signature modelling. In: F. D. Carsey (Ed.). *Microwave remote sensing of sea ice, Geophysical monograph 68* (pp. 137-175). Washington DC: American Geophysical Union.